Wear 368-369 (2016) 26–38

Contents lists available at ScienceDirect

Wear

journal homepage: www.elsevier.com/locate/wear

Evaluation of the effect of temperature on mechanical properties and wear resistance of polyurethane elastomers

H. Ashrafizadeh *, P. Mertiny, A. McDonald

Department of Mechanical Engineering, University of Alberta, Edmonton, Alberta, Canada, T6G 1H9

ARTICLE INFO

Article history:
Received 15 April 2016
Received in revised form
19 August 2016
Accepted 23 August 2016
Available online 30 August 2016

Keywords:
Erosion
Operational temperature
Residual strain
Polyurethane elastomer
Stress softening
Temperature distribution

ABSTRACT

Polyurethane has excellent wear resistance and is an effective protective coating and liner against erosion caused by the impact of solid particles. However, the wear resistance of polyurethane is a function of working temperature due to the influence of heat on its mechanical properties. In this study, an erosion test assembly was designed and developed to evaluate the wear resistance of polyurethane elastomers at controlled temperatures. A cold gas dynamic spray system was used to conduct the erosion tests. The temperature of the exposed front surface of the target material was controlled by adjusting the gas temperature of the cold spray system, and the temperature on the unexposed surface of the samples was kept constant at a desired set-point by the use of a temperature controller, a thermocouple, and cartridge heaters. The transient temperature distribution within the samples was determined by the development of a three-dimensional finite element model. The velocity of the impacting particles was determined by a model based on the principles of supersonic fluid flow through a converging–diverging nozzle. Four polyurethane elastomers with Shore A hardness values of 55–85 were tested. The stress–strain behavior of the polyurethane elastomers *was* characterized at room and elevated temperatures by conducting tensile tests and cyclic loadings. The obtained results showed the substantial effect of testing temperature on erosion resistance of PU elastomers. Comparison of stress–strain behavior of the studied polyurethanes with their erosion resistance at controlled temperatures revealed that the residual strain as a result of plastic deformation and final elongation at break were the key parameters affecting the wear resistance of polyurethane elastomers. Evaluation of the surface morphology of the worn samples confirmed the importance of the residual strain on the erosion resistance of polyurethane elastomers.

1. Introduction

Solid particle erosion is a process in which material is removed from the target surface by the impact of a stream of particles [1]. This type of erosion is a typical wear mode that negatively affects the longevity of parts that are exposed to aggressive erosive environments in many industries including aerospace, marine, mining, wind energy, and oil *and* gas [1–3]. Protective coatings can be employed to increase the lifespan of the equipment exposed to erosive environments. Among all the types of protective coatings, soft elastomeric liners have been found to be effective for industrial use owing to their excellent erosion resistance and comparatively low-cost [4,5]. The excellent erosion resistance of elastomers is a result of their high-resilience and propensity to elastic deformation that allow for absorption of impact energy with minimal plastic deformation [4,6]. Among all the types of elastomeric materials, polyurethane (PU) elastomers have received particular attention given that they can be processed by methods typically used for polymers while still having the superior mechanical properties of vulcanized rubber such as high-elasticity, high-load capacity, and resistance to tear [7]. The relatively low-cost of PU elastomers [7] and the fact that their resistance to wear is greater than that of most polymers [8], rubbers [9], stainless steels [8] and even hard-faced tungsten carbide–cobalt (WC–Co) coatings [10] has made PU an appropriate option for use as protective coatings and liners in large-scale applications *such as* pipelines [11].

Although the relationship between the wear resistance of elastomers and their mechanical properties has been the subject of previous studies, their wear phenomena has been found to be a complex process involving many parameters that affect the final wear performance [4,5]. Ping et al. [10] showed that two PU samples with similar tensile and tear strength had different erosion rates, which was probably due to differences in elongation at break of the two samples. Beck et al. [12] showed that PU samples with similar hardness had different erosion rates. Variation of hysteresis of the samples was presupposed to be the factor

* Corresponding author. fax: +1 780 492 2200.
E-mail address: ashrafiz@ualberta.ca (H. Ashrafizadeh).

http://dx.doi.org/10.1016/j.wear.2016.08.008
0043-1648/

Nomenclature

C_D	Drag coefficient
C_p	Specific heat (J/kg K)
h	Convective heat transfer coefficient (W/m^2 K)
k	Thermal conductivity (W/m K)
$q_s^{''}$	Surface heat flux (W/m^2)
T	Temperature (K)
T_b	Back temperature (K)
T_s	Surface temperature (K)
T_∞	Surrounding temperature (K)
t	Time (s)
V	Velocity (m/s)

Greek symbols

ρ	Density (kg/m^3)

Subscripts

p	Particle condition
g	Gas condition

affecting the erosion rate of the PU. Hysteresis of a polymer represents the fractional energy lost in a deformation cycle. Samples with higher hysteresis had higher erosion rates. Temperature rise caused by the hysteresis of PU samples was suggested to have an effect on the erosion rate of the PU. This would indicate that the variation in temperature due to the higher heat generation could have adversely affected the wear rate of PU elastomers. In a comprehensive study by Li et al. [4], the erosion resistance of a series of castable PU elastomers with almost the same rebound resilience was investigated. A trend of increase in erosion rate with increasing hardness, tensile modulus, and tensile strength was observed. The softest material with the lowest tensile strength produced the maximum resistance to erosive wear. On the other hand, Hutchings et al. [13] showed that there was no simple relation between the wear rate of rubber elastomers and material and mechanical properties such as shore hardness, ultimate tensile elongation, and tensile strength. Rebound resilience was found to be the most dominant factor affecting the wear resistance of rubber elastomers in which the rubber with higher rebound resilience had the highest erosion resistance.

The mechanical properties of PU elastomers are sensitive to temperature and may vary significantly even by changing the temperature by only approximately 50 °C. Thus, the temperature rise during a wear experiment may affect the erosion resistance of PU adversely, and this has been reported in previous studies [3,7,9,12,14–17]. However, the number of studies that have focused on designing a test assembly for studying the effect of working temperature on erosion resistance of PU and, in general, elastomers are limited. Zuev et al. [18] studied the effect of slurry temperature on the erosion rate of rubber elastomers. The erosion rate decreased when the temperature was increased from 20 °C to 70 °C. The increase in elasticity at higher temperatures of the rubber was suggested as the parameter that caused the reduction in the erosion rate. Marei et al. [19] has reported similar phenomenon when evaluating the erosion of rubber in an air blasting test scheme at elevated air temperatures. It was found that the higher the difference between the testing temperature and the glass transition temperature of the rubber, the lower the erosion rate. It should be noted that neither of the aforementioned studies of Zuev et al. [18] and Marei et al. [19] focused on determining the actual temperature distribution within the samples during the erosion test. Hill et al. [14] evaluated the wear performance of PU by employing an abrasion testing procedure. The temperature rise during the abrasion test improved the wear resistance of the elastomer and that outcome was attributed to the softening of PU and its lower hardness at elevated temperatures. On the other hand, in other studies, a decrease in the erosion resistance of PU *was* reported at elevated temperatures [3,9]. Zhang et al. [9] found that the temperature rise caused by the hysteresis decreased the erosion resistance of the PU during the erosion test. Due to the low thermal conductivity of PU, the heat generated by hysteresis caused a temperature rise in the layer beneath the surface. This higher temperature decreased the cohesive energy between the surface layer and the substrate, finally leading to lower erosion resistance. Yang et al. [3] showed that the erosion rate increased by increasing the PU thickness beyond a threshold level. The heat generated that was caused by hysteresis and subsequent temperature rise was found to be responsible for the increase in erosion rate. Although several studies have addressed the effect of temperature on the wear performance of PU elastomers, the number of studies that focused on developing a test assembly for accurate control of the temperature during erosion tests is limited. Further research to study the effect of heat and temperature on wear properties of PU is essential to gain knowledge and greater understanding about the erosion mechanisms of the material at elevated temperatures and identify the key parameters that affect the wear resistance.

The objectives of this study were to (i) design and develop an erosion test assembly capable of controlling the temperature during the wear test, (ii) evaluation of wear resistance of PU elastomers at controlled temperatures and (iii) finding the mechanical properties that best correlate with the erosion resistance of PU elastomers at controlled temperatures.

2. Experimental method

2.1. PU material

The erosive wear resistance of four types of PU elastomers (RoPlasthan-1200-55A, RoPlasthan-1200-85A, RoCoat-3000-85A, and RoCoat-3000M-85A (Castable), Rosen Group, Lingen, Germany) with Shore A hardness within the range of 55–85 was studied. A PU sheet thickness *of* 7 mm was selected to ensure that the thickness did not influence the erosion results and did not decrease significantly during the test [5]. The PU samples were cut into sections of 48 × 36 mm by using a water jet cutter (OMAX 2652 JetMachining Center, OMAX Corporation, Kent, WA, USA). In order to attach the PU samples to the erosion testing equipment, the samples were bonded to aluminum sheets of size 48 × 48 × 3 mm with a thin layer of adhesive (3M DP460, 3M Scotch-Weld, St. Paul, MN, USA). The glass transition temperature of the tested PU elastomers was determined by differential scanning calorimetry (DSC) analysis for the temperature range of −60–180 °C (DSC Q100 V9.8, TA Instruments, New Castle, DE, USA).

2.2. Erosion testing assembly

In order to evaluate the erosion resistance of PU elastomers at controlled temperatures, an erosion test assembly based on ASTM

Standard G76 [20] was developed. The testing equipment was slightly modified from the requirements of ASTM Standard G76 to incorporate the effect of the PU temperature during the erosion test. A cold gas dynamic spray system ("cold spray") (SST Series P, CenterLine Ltd., Windsor, ON, Canada) was used to heat and move compressed air at various temperatures, and the gas was used to accelerate the erodant particles to impact on the surface of the PU. The operating parameters of the cold spray system that were employed for erosion testing are summarized in Table 1. The PU sample holder was fabricated from copper and it was equipped with two cartridge heaters (50 W Miniature High Temperature Cartridge Heater (D 1/8″ × 1 1/4″), McMaster-Carr, Aurora, OH, USA). A temperature controller (CNI8A42, Omega Engineering Inc., Stamford, CT, USA) was used to maintain the temperature of the copper cube at the desired set-point. Fig. 1 shows a schematic and the assembly of the custom-fabricated erosion testing system. As shown in this figure, the erosion tests were conducted at an impact angle of 30° given that this angle is close to conditions typically found in practice [3] and also from the fact that the maximum erosion of ductile materials, including elastomers, occur at an impact angle of 30° [5,15].

Table 1
Cold spray system parameters.

Pressure of compressed air (kPa)	435
Temperature of compressed air (°C)	25, 75, and 125
Stand-off distance (mm)	22
Nozzle length (mm)	70
Nozzle throat diameter (mm)	2.5
Nozzle output diameter (mm)	5.4

The PU samples were weighed before and after the erosion test by a balance with an accuracy of ± 1 mg (Adventurer Pro AV313, OHAUS Corporation, Parsippany, NJ, USA). The wear rate was calculated by normalizing the mass loss of the sample with the mass of the erodant particles. Garnet sand (Super Garnet, V.V. Mineral, Tamil Nadu, India) was chosen as the erodant medium. Fig. 2 shows the morphology of the garnet sand. As observed in the image, the sand particles are rounded on the sides. The average diameter of the garnet sand particles was measured by image analysis (ImagePro, Media Cybernetics, Bethesda, MD, USA). The average diameter was calculated by averaging length of lines passing through the object centroid at 2° intervals. The average size of the garnet sand particles was 266 ± 49 μm (n=159). In this study the number of measurements (n) and the standard deviation are always presented with average values.

Each type of PU was tested at three different set-point temperature values for conditions A, B, and C (see Table 2). The erosion resistance of a minimum of two samples was evaluated for each condition. The standard deviation was calculated and reported for cases where more than two samples were tested. The PU samples were heated by both the hot compressed air from the cold spray system and by the cartridge heaters that were mounted in the copper plate support. Details on the set-point temperatures of the air from the cold spray system and in the copper support plate are summarized in Table 2. The PU samples were preheated for 120 s from the unexposed surface by the cartridge heaters and copper plate. Then, the samples were heated at the exposed surface with air from the cold spray system (see Fig. 1) for 120 s, simultaneously with heating from the unexposed surface that was in contact with the copper plate support. This ensured that the temperature was

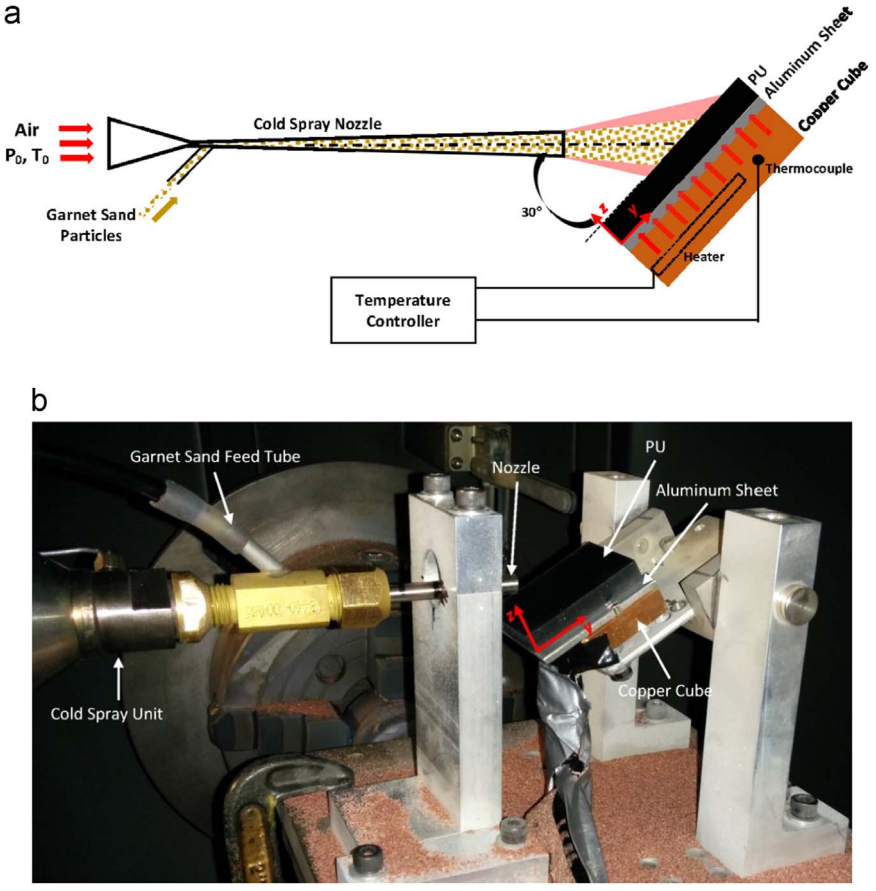

Fig. 1. (a) Schematic and (b) image of the custom-made erosion test assembly.

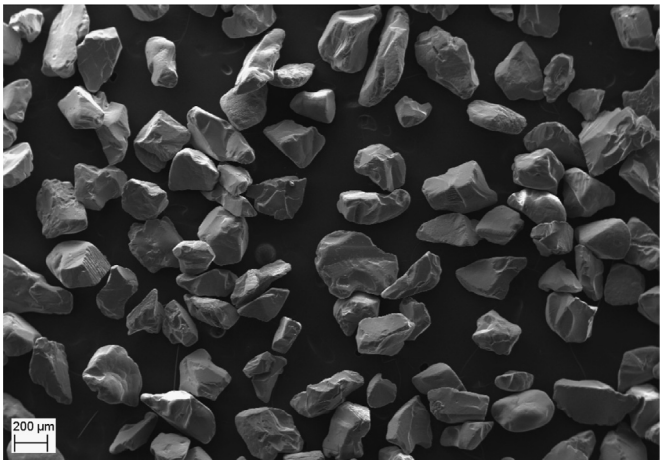

Fig. 2. Morphology of the garnet sand particles.

Table 2
Details parameters for each testing condition of the PU samples.

Test condition Parameters	Condition A	Condition B	Condition C
Target PU temperature (°C)	22	60	100
Pressure of air (kPa)	435	435	435
Set temperature at cold spray console (°C)	25	75	125
Set temperature at temperature controller (°C)	25	65	105
Preheating period from the unexposed surface (s)	120	120	120
Preheating period from the unexposed and exposed surfaces (s)	120	120	120
Erosion test period (s)	240	240	240

uniform throughout the PU samples prior to initiating the erosion tests.

2.3. Temperature measurements

A J-type thermocouple (Gage 30, Thermo Electric Ltd., Brampton, ON, Canada) was inserted into the PU substrate at a depth of 1.5 mm below the surface of the center of the area that was to be eroded. A data acquisition system (SCXI 1600, National Instruments, Austin, TX, USA) was used to collect the data of transient temperature that was measured by the inserted thermocouple. The data obtained from this thermocouple were used for the verification of the subsequently presented finite element (FE) heat transfer model and to study the possible temperature rise caused by friction forces and hysteresis during the erosion process. The temperature at the unexposed surface of the PU samples was measured by a second J-type thermocouple of the same type that was placed below the unexposed surface between the PU and aluminum sheet. An infrared camera (VIR50, Extech Instruments Corporation, Nashua, NH, USA) was employed to measure the temperature of the exposed surface of the PU samples. The exposed surface of the PU was divided into 12 square sections and the temperature at each section was measured by pointing the infrared camera towards the center of a given section. Three measurements were conducted for each section and at a given testing condition. The data obtained were averaged and was used to formulate boundary conditions for the FE model. The emissivity needed for the setup of the infrared thermometer pointing towards the PU surface was determined by adjusting the emissivity coefficient until approximately the same temperature was measured by the infrared thermometer and the thermocouple that was inserted below the sample surface. The emissivity was determined as 0.99.

2.4. Materials and mechanical testing

The stress–strain behavior of the PU samples at room and elevated temperatures were studied by conducting tensile tests and cyclic loading. PU sheets with a thickness of 1 mm were cut to shape and dimensions based on the ASTM Standard D638-Type V [21] by waterjet cutting (OMAX 2652 JetMachining Center, OMAX Corporation, Kent, WA, USA). A dynamic mechanical analyzer (ElectroForce 3200, TA Instruments, Eden Prairie, MN, USA) was employed to conduct the tensile tests and cyclic loadings. The tensile tests were conducted up to a nominal strain of 350% in the PU while cyclic loading was performed for a nominal strain range of 0–50%. The tests were conducted at 25 °C and at elevated temperatures of 60 °C and 100 °C at a strain rate of 0.25 s^{-1}. Three samples were tested for every experiment. In the elevated temperature experiments the samples were preheated for 4 min at the desired temperature to ensure that the temperature within the samples was uniform prior to testing.

2.5. Scanning electron microscopy

The surface topography of the worn PU elastomers were examined by using a scanning electron microscope (EVO LS15 EP, Carl Zeiss Canada Ltd., Toronto, ON, Canada) in the secondary electron mode with a beam voltage of 5 kV. A thin film of carbon was deposited onto the PU surface by using a carbon evaporation system (EM SCD 005, Leica Baltec Instrument, Balzers, Liechtenstein) to avoid surface charging during scanning electron microscopy (SEM).

3. Mathematical model for determination of erodant particle impact velocity

The velocity of the erodant particles at the nozzle exit was determined by employing a mathematical model that is based on the principles of dynamics and thermodynamics of compressible fluid flow through a converging–diverging nozzle [22,23]. In this model, the Mach number at each point was determined based on the geometry of the nozzle. The Mach number at a given cross-sectional area, along with the appropriate governing thermodynamic equations and equations of motion for a compressible isentropic fluid flowing through a converging–diverging nozzle, was used to calculate the pressure, velocity, temperature, and density of the gas at that point [22,23]. The particle velocity was determined according to the second law of motion, assuming that the drag force was the only force that was applied on the accelerating particles. Details regarding the equations and experimental validation of the mathematical model can be found elsewhere [22–25].

Euler's numerical integration method was used to solve the equation of motion, and the final equation for particle velocity through the nozzle axis was determined as [26]:

$$V_{p,\,x} = \left(V_{p,\,x-1}^2 + \frac{1.5\Delta x C_D \rho_g}{d_p \rho_p} \left(V_g - V_{p,\,x-1}\right)^2 \right)^{0.5}, \quad (1)$$

where V_p, V_g, d_p ρ_p, ρ_g, and C_D are particle velocity, gas velocity, particle diameter, particle density, air density, and drag coefficient, respectively. Eq. (1) was solved at spatial intervals of $\Delta x = 0.1$ mm through the length of the nozzle. The average diameter of the

garnet sand particles (266 μm) and a density of 4 g/cm^3 [27] were used in conjunction with Eq. (1).

4. Finite element model simulation

In order to determine the transient temperature field within the PU samples during **an** erosion test, a thermal finite element (FE) model was developed using the generalized FE software ABAQUS/Standard Version 6.13 [28]. Boundary conditions of the model were assigned according to the preheating that was introduced at the exposed and unexposed surfaces of the PU sample. The erosion tests were conducted in a dust collection system that produced airflow with a velocity of approximately 1.4 m/s over the sample surface during the first step of preheating. This flow of air produced forced convection heat transfer from the surface during the initial 120 seconds of preheating where the samples were being heated from the unexposed surface. Thus, for the first 120 seconds of the preheating procedure, the boundary conditions were selected as a transient temperature on the unexposed surface **(T_b)** of the samples and forced convection on the top surface. The heat transfer coefficient was determined according to Newtons' law of cooling under steady-state conditions [29] as $h = 53 \pm 2$ W/m^{2}K ($n = 3$) for three set-point temperatures of 60 °C, 80 °C and 105 °C on the unexposed surface of the samples.

In the second preheating step, the boundary condition on the unexposed surface of the sample was similar to that of the first preheating stage (as transient temperature measured by the thermocouple) while the boundary condition on the exposed surface was changed from a convection boundary condition to a temperature boundary condition, with the temperature being measured with the infrared camera **(T_s)**. Given that the effect of heat generation caused by friction **from** the impacting particles and repeated deformation of PU was neglected, the boundary conditions during the erosion test remained unchanged and were similar to those of the second step of preheating. The validity of this assumption was verified by monitoring the temperature measured by the thermocouple that was inserted 1.5 mm below the PU surface during the erosion test. Constant thermal properties such as thermal conductivity and negligible heat loss due to natural convection from the sides of the sample were the other two assumptions that were made during the development of the FE model. The governing equation that was solved by the finite element model was

$$\rho C_P \frac{\partial T}{\partial t} = div(k\ grad(T)), \tag{2}$$

where ρ, C_p, T, and k represent density, specific heat, temperature, and thermal conductivity, respectively. The Galerkin method was then used to derive the integral form of the heat transfer equation, yielding the finite element equations in matrix form. A standard heat transfer protocol in the ABAQUS software was chosen for the analysis. In the chosen formulation, the time integration was completed by the backward Euler method (Crank–Nicholson operator) [28]. Three-dimensional eight-node linear heat transfer brick elements (DC3D8 in the ABAQUS library) were selected as the element type [28]. The model was discretized with 13,824 elements. The initial condition and boundary conditions were defined based on the discussed preheating stages as:

$$T(x,\ y,\ z,\ t=0) = T_{initial}, \tag{3}$$

$$T(x,\ y,\ z=0,\ t) = T_b(t), \tag{4}$$

$$q_s'' = (T_\infty - T(x,\ y,\ z=l,\ t))h \quad \text{for} \quad t < 120\ \text{s}, \tag{5a}$$

$$T(x,\ y,\ z=l,\ t) = T_s(x,\ y,\ t) \quad \text{for} \quad t > 120\ \text{s}. \tag{5b}$$

5. Results and discussion

5.1. Erodant particle velocity

The velocity of air flowing through the nozzle and, therefore, the particle velocity, is a function of temperature and pressure of the gas as set at the cold spray console. As shown in Table 2, for all the testing conditions, the gas pressure was kept constant while the set temperature at the cold spray console was increased from 25 °C to 125 °C for Conditions A–C. The gas at higher temperatures has higher kinetic energy and velocity, which affects the velocity of the fed particles. Table 3 summarizes the particle exit velocity that was estimated for each set temperature. As shown in the table, the particle velocity increased when the gas temperature was increased. To ensure that a small deviation in velocity alone did not significantly affect the erosion rate, the wear performance of a material with erosion resistance that is insensitive to the temperatures in the range explored in this study was tested. Aluminum sheets were selected for that purpose given that the mechanical properties of aluminum do not vary appreciably within the given temperature range. The erosion performance of the aluminum samples were tested at 25 °C and 100 °C. The results revealed that the erosion rate, as expressed as a ratio of mass loss of aluminum to mass of impacting garnet particles, did not vary noticeably within the temperature range that was studied (see Table 4). The two-sample *t*-test statistical method was employed to verify whether or not the average mean of the two groups shown in Table 4 were significantly different. The *p*-value for the *t*-test was based on the assumption of equal variances and was calculated to be 0.34. Given that the calculated *p*-value is higher than 0.05, it cannot be concluded that there is a significant difference between the average values of the two groups. This suggests that while the variation of temperature of the gas as set at the cold spray console affects the temperature distribution within the target samples, its effect on velocity of the garnet sand particle is negligible.

5.2. Temperature distribution within the PU samples

The validity of the FE heat transfer model that was developed for determining the temperature distribution was evaluated by comparing the predicted temperature from the model with that of the experimental data obtained from the J-type thermocouple that was inserted 1.5 mm below the surface. Fig. 3 shows the experimental results obtained from the thermocouple along with the modeling data for conditions B and C (see Table 1**).** The difference between the temperature measured by the thermocouple and that obtained from the simulation after 120 s is most probably due to inaccuracies in measuring the surface temperature by the infrared camera. The infrared camera measures the average temperature of a surface area with an approximate diameter of 12 mm while the local temperature on the top of the thermocouple could have been higher in value. Irrespective of this deviation, there was good agreement between the simulation and the experimental results,

Table 3
Garnet sand particle velocities at the nozzle exit for different gas temperatures.

Gas set temperature at cold spray console (T_0) (°C)	Gas set pressure at cold spray console (P_0) (psig)	Calculated particle velocity and nozzle exit (m/s)
25	50	73
75	50	76
125	50	78

which thus verifies the model. Fig. 3 also shows that after 240 s (end of preheating), a steady-state condition was practically achieved and the temperature did not vary appreciably beyond that time.

The model was then employed to determine the temperature distribution within the PU samples during the erosion tests. The temperature field calculated by the FE model, as shown by the example in Fig. 4, was employed to determine the temperature distribution after 240 s of preheating. As seen in Fig. 4, the temperature in the to-be-eroded area was relatively uniform and was determined by the FE simulation to be close to 60 °C and 100 °C for erosion testing conditions B and C, respectively. The temperature distribution within the PU samples during the erosion tests was similar to that of the end of the preheating stage given that the data obtained from the thermocouple that was located below the surface confirmed a negligible temperature rise caused by friction and the deformation of PU.

Table 4
Non-dimensional erosion rate of aluminum samples at different air temperatures.

Gas set temperature at cold spray console (T_0) (°C)	Gas set pressure at cold spray console (P_0) (psig)	Erosion rate (mg/g)
25	50	0.37 ± 0.01 ($n=6$)
125	50	0.38 ± 0.01 ($n=5$)

5.3. Erosion rates of PU at the set temperatures

Table 5 summarizes the measured glass transition temperatures of the PU elastomers that were studied. As can be seen, all the PU elastomers were in their rubbery phase at room temperature (25 °C). The erosion resistance of the PU elastomers was evaluated at 25 °C and at other elevated temperatures that are presented in Table 2. Fig. 5 shows the non-dimensional erosion rate for the four types of PU elastomers that were tested at the various temperatures. Standard deviations are presented as error bars in Fig. 5 for data points where more than two samples have

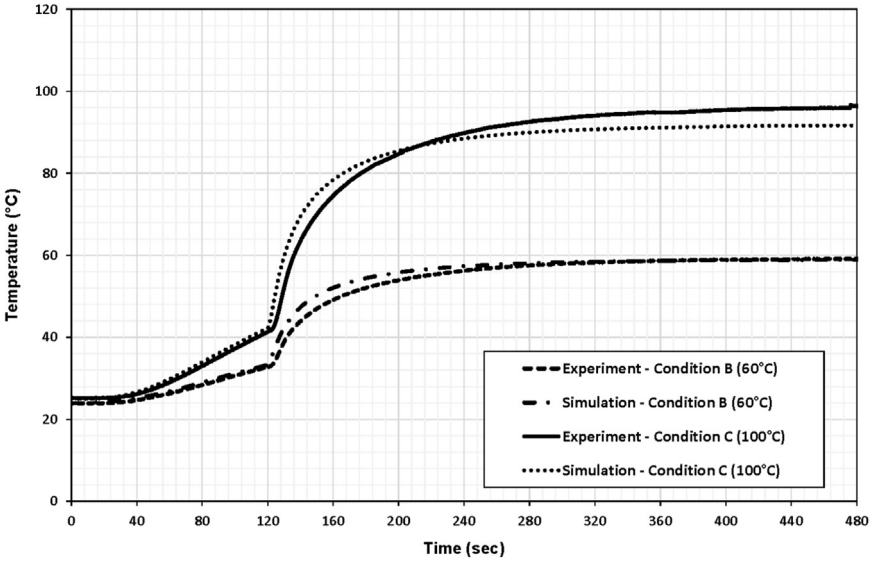

Fig. 3. Transient temperature at 1.5 mm below the surface of the PU sample – experiment and model.

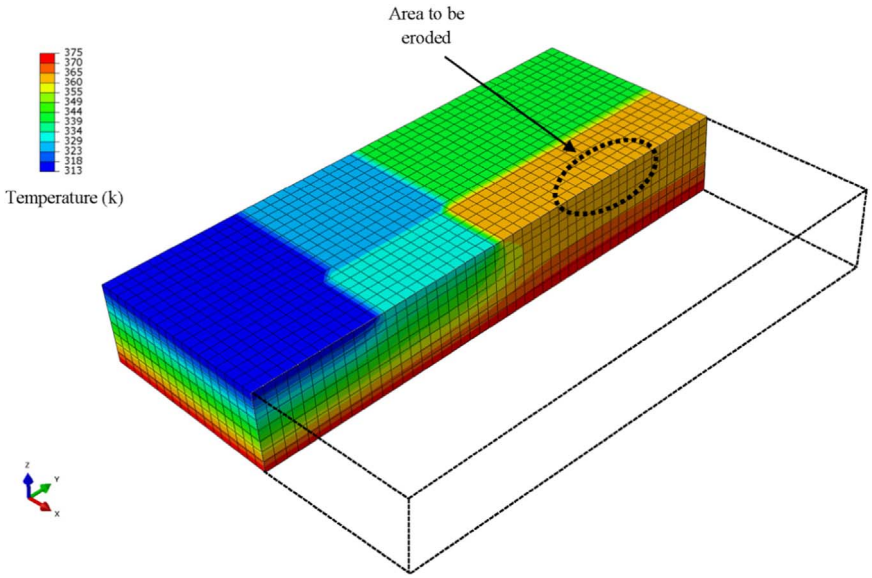

Fig. 4. Temperature distribution within PU for condition C (100 °C) test procedures after preheating and before the erosion tests.

been tested. The small values of the standard deviations shown in Fig. 5 indicate excellent repeatability of the erosion testing assembly that was developed. The erosion rate of 1200-55A and 1200-85A PU elastomers increased continuously from 0.016 to 0.069 mg/g and 0.036 to 0.086 mg/g, respectively, within the range of 25–100 °C. On the other hand, for the 3000 PU series, 3000-85A and 3000M-85A the trend was different, and an initial improvement of wear resistance, as evidenced by the decrease in erosion rate (see Fig. 5), occurred up to 60 °C. The erosion rate increased beyond 60 °C for all investigated PU elastomers. The results shown in Fig. 5 indicate that even with variation of temperature within the range of 20–60 °C, significant changes in erosion resistance of the PU elastomers can occur. The fact that the changes in wear resistance of the studied PU elastomers were not similar as the PU temperature was varied, emphasizes the influence of the PU temperature on its wear resistance.

Tensile and cyclic loading tests were conducted to explain the trends observed in Fig. 5. The stress–strain curves obtained from these experiments were used to study the changes in mechanical properties of PU as a result of temperature rise and its corresponding influence on wear resistance. Fig. 6 shows the stress–strain curves obtained from tensile testing at room and elevated temperatures for strains up to 350%. The graph indicates that all the PU elastomers became softer with increasing temperature. This softening was a result of crosslinking disruption and breakage of some hydrogen bonds at higher temperatures and reduction in crosslinking of the polymer structure [30,31]. A comparison of Figs. 5 and 6 shows that the softness of the PU elastomer is not the only factor that affects the erosion rate. Although the 1200-55A PU grade is the softest elastomer, the 3000M-85A and 3000-85A elastomers have lower erosion rates at 60 °C. This suggests that another parameter, other than the softness of the PU, has affected the elastomer wear resistance. The data obtained from tensile tests were also used to calculate the ultimate strength and elongation at break of the PU elastomers that failed at strains lower than 350%. These data are summarized in Table 6. The fact that the 3000 PU series have lower elongation at break and lower failure stresses at 60 °C compared to those of the 1200 series suggests that although the final elongation at break may have an impact on the final erosion resistance of the elastomers, it is not the only parameter that affects their wear performance.

Most polymer-based materials, including PU elastomers, experience plastic deformation alongside with elastic behavior upon deformation. This plastic deformation can contribute to the formation of a permanent set (residual strain) upon unloading and also stress–strain hysteresis. The plastic deformation in PU elastomers is a result of the irreversible breakage-disruption of the chemical structure and changes in the orientation of the hard-soft phase [31]. The load induced by the impact of erodant particles during the erosion process is similar to repeated loading–unloading cycles. Consequently, the evaluation of the PU behavior during cyclic loadings can provide important information about the ability of the material to regain its initial condition. Fig. 7 shows the stress–strain curves of the initial loading-unloading cycle of the PU elastomers that were studied. Qualitatively, for all tests, the PU material became softer and the hysteresis loop decreased at higher temperatures. However, for the case of the 3000 PU series and, in particular, 3000M-85A, the PU exhibited extensively different behavior; the permanent set and hysteresis loop became smaller as the temperature increased (see Fig. 7d). On the other hand, for the 1200-55A and 1200-85A PU samples, the permanent set and material behavior did not greatly vary by increasing the temperature. To obtain a quantitative evaluation of the effect of temperature on the residual strain of PU, the residual strain of at least three samples during a loading-unloading cycle was measured as presented in Table 7. The graph shows that the maximum reduction in permanent set occurred in the 3000M-85A and 3000-85A PU. A comparison of the permanent set data shown in Table 7 with the erosion results at various temperatures in Fig. 5 reveals that there is a correlation between the ability of the material to regain its initial condition and the erosion resistance. 3000M-85A and 3000-85A PU elastomers that experienced a reduction in permanent set by increasing the temperature from 25 °C to 60 °C exhibited improved wear resistance at 60 °C (see Fig. 5). This behavior is most probably due to the fact that for

Table 5
Commercial name and glass transition temperature of PU elastomers.

PU commercial name	Glass transition temperature (°C)
RoPlasthan-1200-55A	−24
RoPlasthan-1200-85A	−19
RoCoat-3000-85A	−6
RoCoat-3000M-85A	10

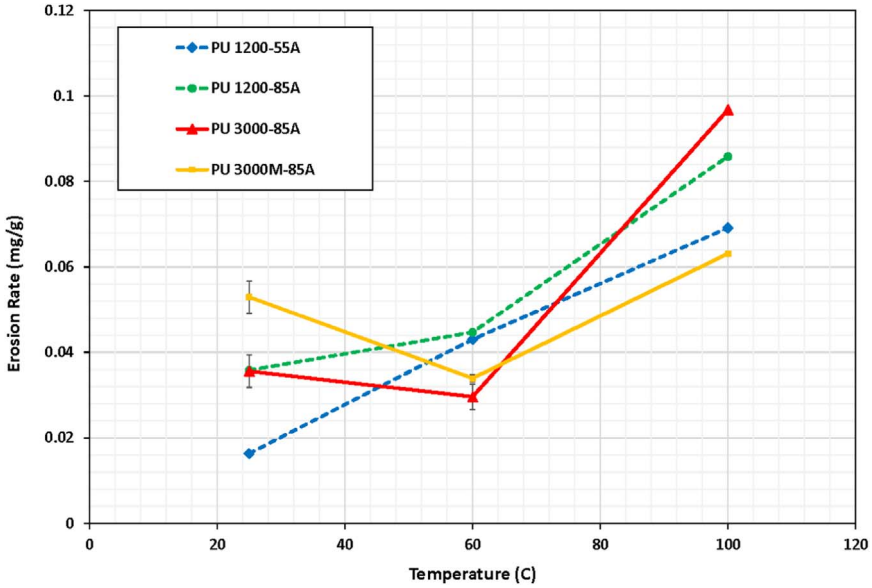

Fig. 5. Erosion rate as a function of PU temperature.

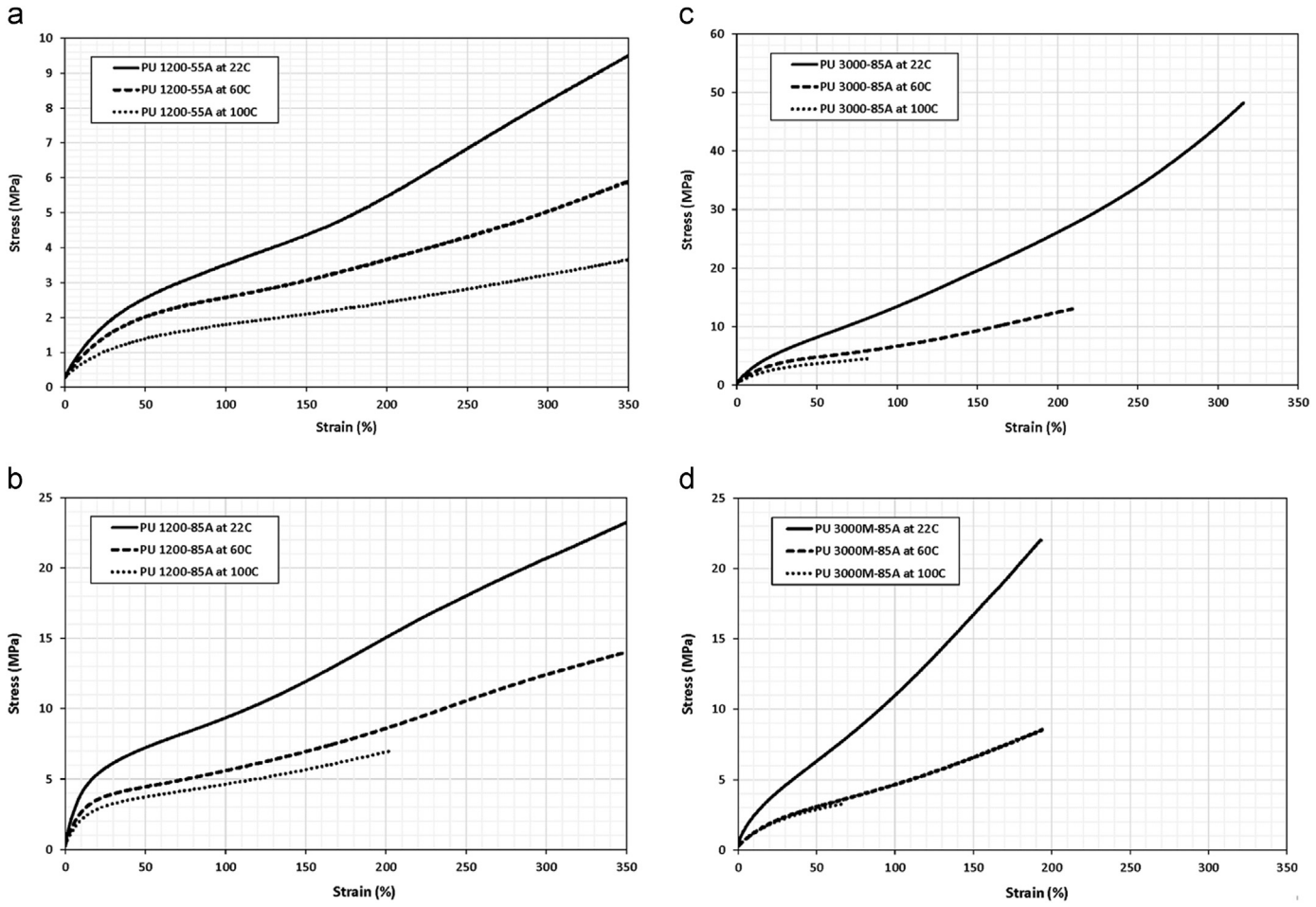

Fig. 6. Stress–strain curves obtained at various test temperatures for elongation up to 350% for (a) 1200-55A, (b) 1200-85A, (c) 3000-85A, and (d) 3000M-85A PU elastomers.

Table 6
Nominal stress and strain failure data of PU elastomers up to a nominal strain of 350%.

Temperature (°C)	25 °C		60 °C		100 °C	
PU type	**Ultimate stress (MPa)**	**Elongation at break (%)**	**Ultimate stress (MPa)**	**Elongation at break (%)**	**Ultimate stress (MPa)**	**Elongation at break (%)**
1200-55A	NA	NA	NA	NA	NA	NA
1200-85A	NA	NA	NA	NA	6.4 ± 0.5 (n = 3)	188 ± 16 (n = 3)
3000-85A	44.7 ± 3.4 (n=3)	304 ± 12 (n=3)	13.9 ± 1.8 (n=3)	225 ± 30 (n=3)	4.2 ± 0.2 (n=3)	77 ± 6 (n=3)
3000M-85A	24.7 ± 3.0 (n=3)	210 ± 18 (n=3)	8.8 ± 1.0 (n=3)	200 ± 11 (n=3)	3.1 ± 0.1 (n=3)	58 ± 7 (n=3)

conditions and PU in which lower permanent set occurred, a higher number of impacts is needed in order to deform the surface up to the threshold strain for final detachment of fragments of material from the surface. On the other hand, at the set temperature of 100 °C, although the permanent set tends to decrease further, the significant reduction in material strength (see Table 6) has adversely affected the erosion resistance of the PU elastomers.

In PU elastomers, plastic deformation as a result of irreversible breakage of some crosslinks can occur upon initial loading. Thus, during the first loading cycle, the PU exhibits higher strength to deformation ratio while upon second loading the material will already be permanently deformed due to the damage induced in the microstructure of the PU during the first loading. The level of stress softening of PU can have a direct impact on the erosion resistance of the PU given that the stress softening that occurs due to the impact of particles would result in higher strains upon impact of subsequent particles with similar impact force during the erosion process. In fact, the impact of previous erodant particles would weaken the target material by introducing permanent damage in the mechanical structure of the elastomer. To evaluate the level of stress-softening of the studied PU elastomers, cyclic loading tests similar to those presented in Fig. 8 were conducted and a parameter known as Mullins factor was calculated [31]. The Mullins factor provides information about how much the second loading deviates from the first loading in terms of hyperelastic response, which is defined as [31]:

$$\text{Mullins factor} = 1 - \frac{\text{Energy loss of second load} - \text{unload cycle}}{\text{work required to extend the PU to the desired strain}}. \quad (6)$$

The energy loss of the second load–unload cycle and the work required to deform the PU to the desired strain are equivalent to the area under the hysteresis loop of the second cycle and the area below the loading curve of the first cycle in the stress–strain

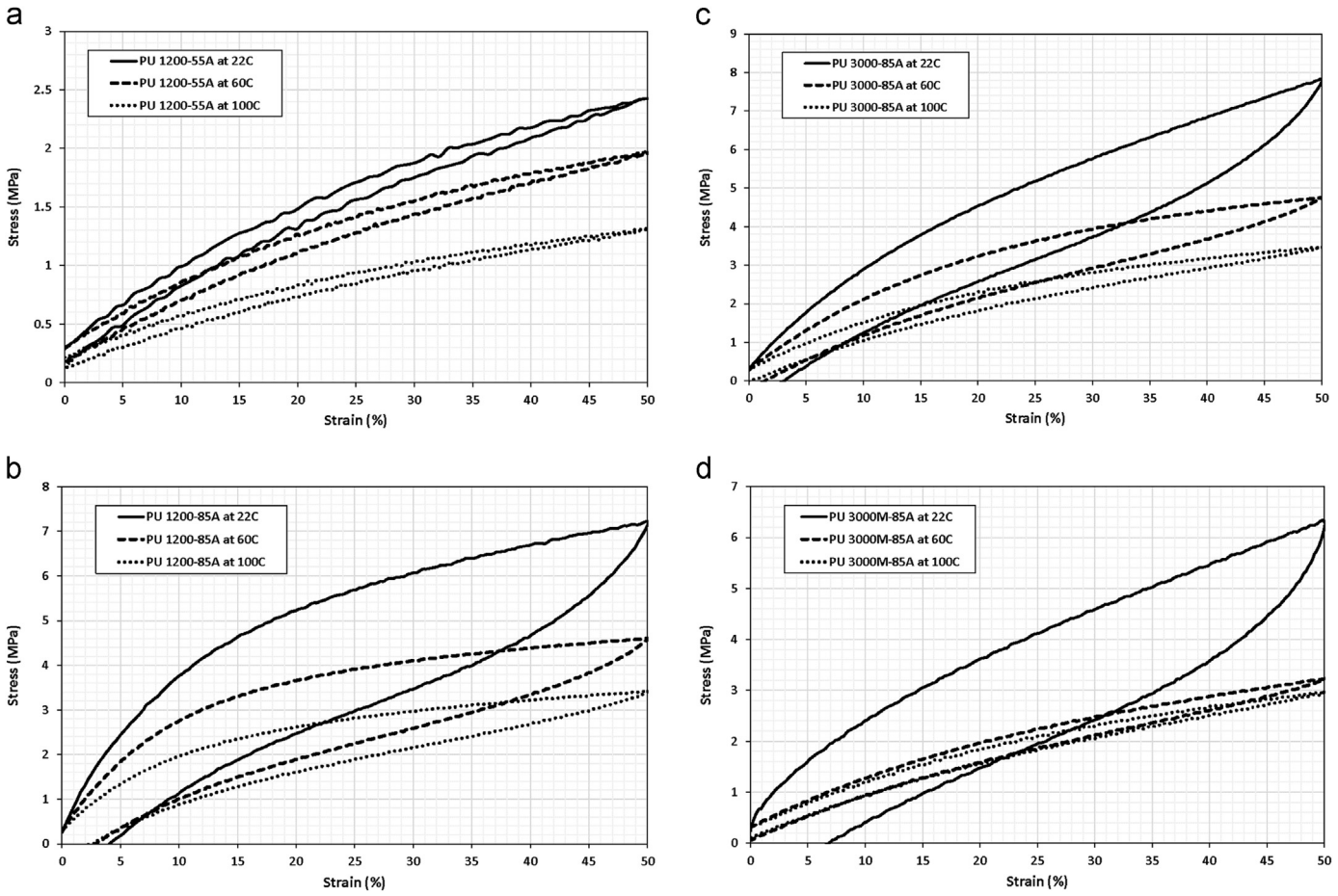

Fig. 7. First cycle of loading-unloading at various temperatures for elongation up to 50% for (a) 1200-55A, (b) 1200-85A, (c) 3000-85A, and (d) 3000M-85A PU elastomers.

Table 7
Permanent set of PU elastomers after loading up to 50% nominal strain at various temperatures.

Temperature (°C) PU type	25 °C Permanent set (%)	60 °C Permanent set (%)	100 °C Permanent set (%)
1200-55A	Less than 0.1% ($n=4$)	Less than 0.1% ($n=4$)	Less than 0.1% ($n=4$)
1200-85A	4.2 ± 0.1 ($n=3$)	2.9 ± 0.1 ($n=3$)	2.4 ± 0.4 ($n=3$)
3000-85A	3.1 ± 0.1 ($n=3$)	1.4 ± 0 ($n=3$)	0.2 ± 0.2 ($n=4$)
3000M-85A	7.1 ± 0.7 ($n=4$)	Less than 0.1% ($n=3$)	Less than 0.1% ($n=4$)

curves, respectively. The closer the Mullins factor is to unity, the closer the PU elastomer is to an ideal Mullins response, that is, the reloading stress–strain is closer to the previous unloading path. In this study, numerical integration was employed to calculate the area below the stress–strain curve for determination of the Mullins factor. Fig. 9 shows the calculated Mullins factor for PU elastomers at the set temperatures. As can be seen, the Mullins factor remained almost unchanged for the 1200-55A PU while it increased with temperature for all the other PU elastomers that were studied. The rate of increase of the Mullins factor for the 3000-85 A and 3000M-85A PU elastomers was higher from 25 °C to 60 °C. A Mullins factor value that was closer to unity indicates that more damage will be introduced to the PU upon impact of each erodant particle. A comparison of Fig. 9 with that of erosion rates of the PU elastomers at various temperatures (see Fig. 5) suggests that the decrease in the erosion rate of 3000-85A and 3000M-85A PU at 60 °C is related to the softness and lower plastic deformation (see Table 7) of these elastomers at 60 °C.

5.4. Evaluation of the worn surfaces

The erosion mechanism of elastomers is a function of the wear testing procedure (erosion or abrasion), properties of abrasive media, erodent velocity and mechanical properties of the target material. The wear mechanisms that have been suggested for elastomers are:

a) The formation of cracks below the worn surface due to the tensile, compressive, and shear stresses caused by the impact of particles and final detachment of fragments as a result of the intersection and extension of the formed cracks [3,7,9,32];
b) The formation of asperities by plastic deformation to produce ridges perpendicular to the direction of impact and final fracture of the deformed asperities [5,12–14,17,33,34]; and
c) Random scratches and gouges on worn surfaces due to the cutting and gouging by angular grit media [12,35].

Evaluation of the eroded surfaces of PU elastomers suggests that the erosion mechanism was plastic deformation of the surface and the development of asperities and ridges perpendicular to the direction of impact. Fig. 10 shows the surface of 1200-55A PU elastomer samples that were eroded at room and elevated temperature. In the PU sample that was held at 25 °C (see Fig. 10a), the worn surface showed deformed asperities while at elevated temperatures, where the erosion rate was higher, ridges perpendicular to the impact direction were formed (see Fig. 10b and c). A similar

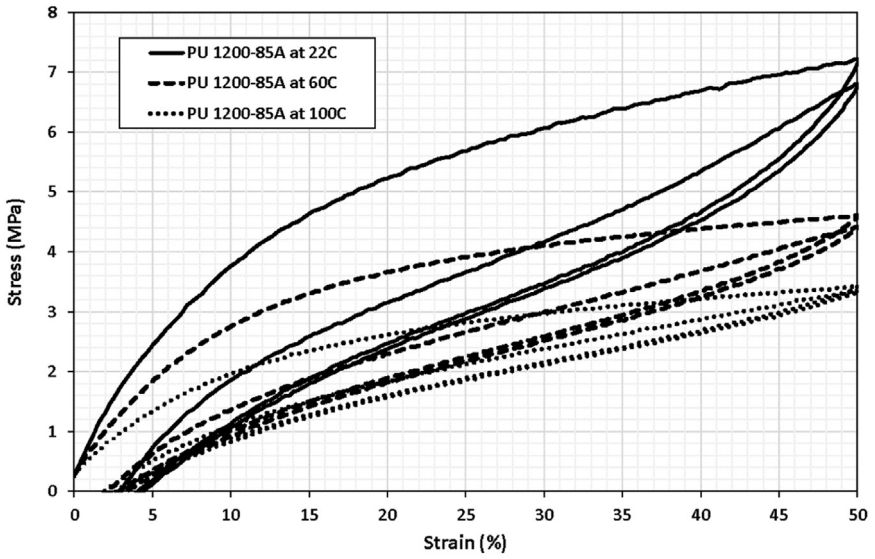

Fig. 8. First and second cycles of loading–unloading at various temperatures for elongations up to 50% for 1200-85A PU elastomer.

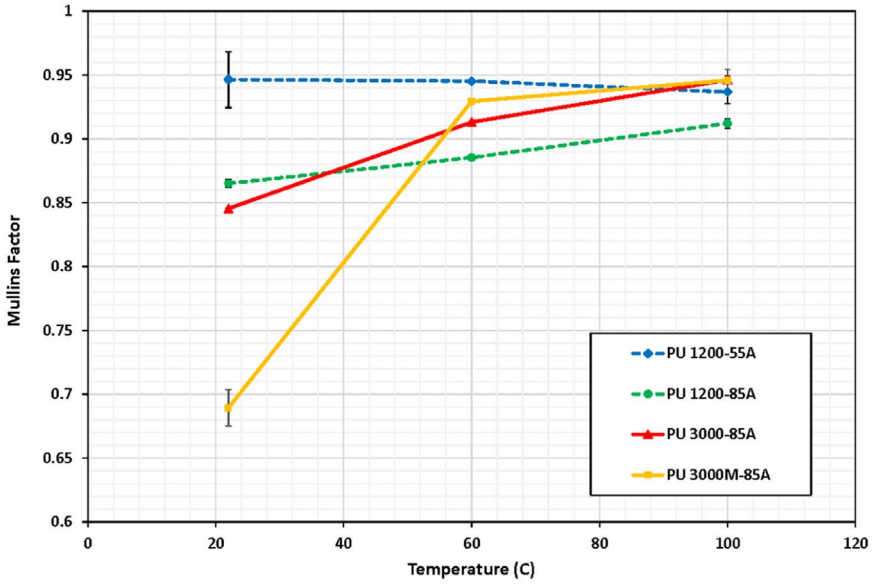

Fig. 9. Mullins factor of PU elastomers as a function of temperature.

behavior was observed for the 1200-85A PU: asperities emerged at 25 °C and ridges developed perpendicular to the impact direction at elevated temperatures. Although the mechanism of formation of these ridges and subsequent erosion as a result of detachment of these ridges have been discussed in previous studies [5,14,33], side view images that can distinctly show the morphology of these ridges are limited. To that end, SEM images were captured for the condition that the PU sample was slightly angled with respect to the SEM detector. These images are shown in Fig. 11, which show that the asperities that protrude from the surface were formed against the impact direction of the erodant particles (shown by an arrow). The asperities were generated as a result of plastic strain induced by particle impact. The accumulation of strain due to subsequent impact led to the deformation of the asperities to values such that cracks were formed on the bottom of the asperities, followed by the final detachment of the material. A typical crack produced **at** the base of one of these asperities is indicated in Fig. 11a by a circle. On the other hand, the partially detached, but stretched material shown in Fig. 11b (marked by circles) provides further support for the proposed erosion mechanism and the importance of elongation at break on the erosion resistance of PU caused by solid particle impact. In PU elastomers with lower elongation at break, the deformed asperities on the target surface detached easier from the surface that would lead to higher mass loss and, therefore, higher erosion rate.

The morphology of the eroded surfaces of 3000-85A (see Fig. 12) and 3000M-85A PU (see Fig. 13) was slightly different from that observed in Fig. 10. The asperities that were formed on the 3000 series PU were smaller in size and the ridges were not as continuous and as large as the ones formed on the 1200-55A and 1200-85A PU elastomers. This behavior was due to the smaller elongation at break of the 3000 series (see Table 6) which led to the detachment of asperities at lower strain. Thus, the asperities have detached from the surface before extending to large strain values as was observed for the 1200 series PU (see Fig. 10). In addition, in contrast to the 1200 series PU, the surface morphology of the 3000 series PU that was tested at 100 °C was different from those samples that were tested at 25 °C and 60 °C. The asperities were smaller compared to those samples held at 25 °C and 60 °C, and continuous ridges were observed (see Figs. 12c and 13c).

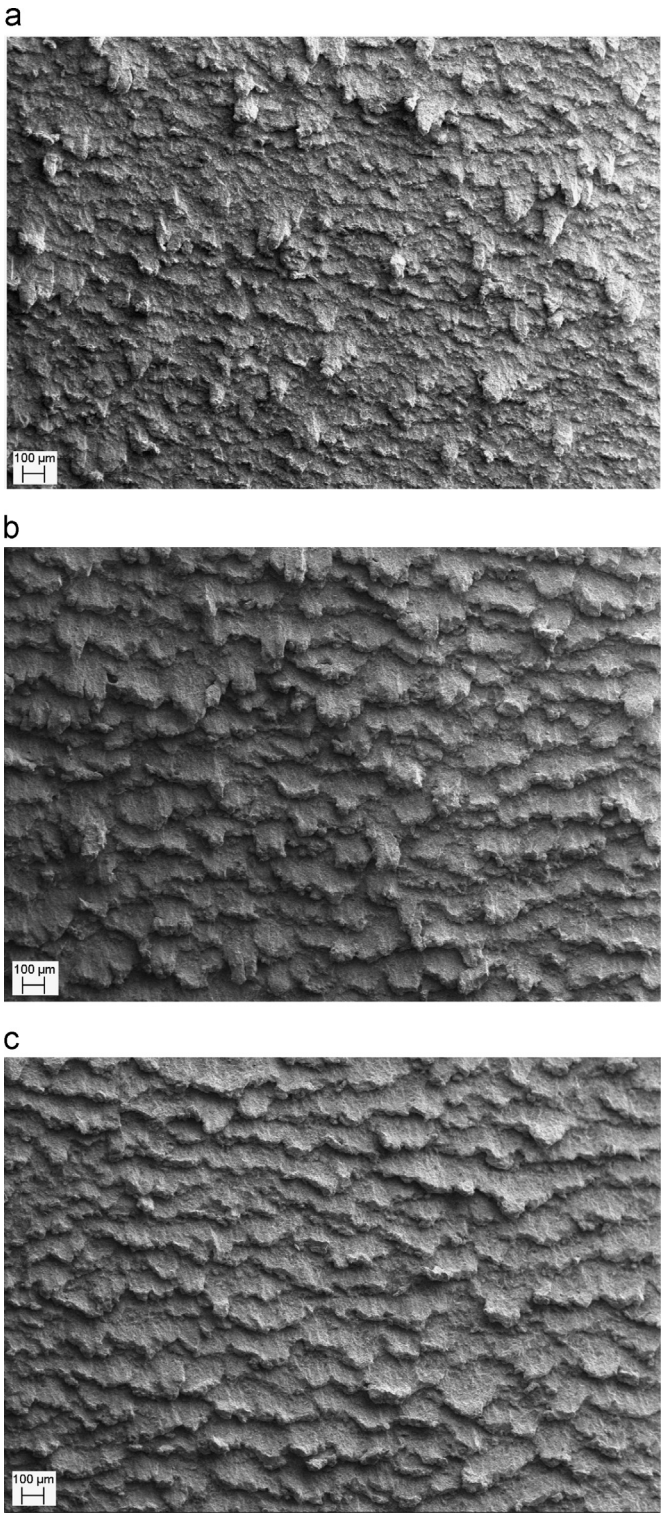

Fig. 10. SEM images of eroded 1200-55A PU surface at (a) 25 °C, (b) 60 °C, and (c) 100 °C.

This behavior was most probably due to the significant reduction in elongation at break and ultimate strength of the 3000 series PU elastomers at 100 °C as was shown in Table 6. This behavior suggests that although there is no simple relation between elongation at break and the erosion rate, the surface topography and the wear resistance of the PU are dependent on the elongation at break. It should be noted that the spherical shape defects observed in Fig. 13 are cavities that were formed in the PU elastomer during its

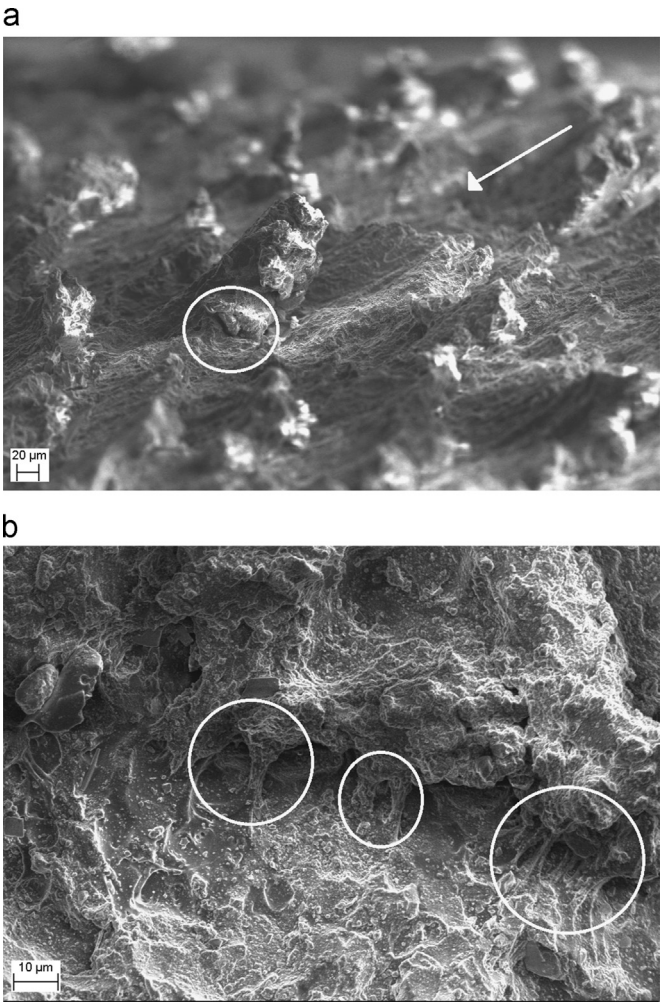

Fig. 11. SEM images of eroded 1200-55A PU surfaces tested at 60 °C: (a) side and (b) top view.

fabrication as a result of possible air entrapment and formation of gases during curing. Two of this typical spherical shape defects on the surface of PU are shown by arrows in Fig. 13a.

The evaluation of the erosion mechanism of the PU elastomers that were held at various temperatures and eroded, not only revealed how temperature affects the erosion mechanism, but close evaluation of the worn surfaces also provided further support of the aforementioned effect of the permanent set and elongation at break on the erosion resistance of PU elastomers. The 1200-55A PU exhibited the minimum erosion rate at 25 °C (see Fig. 5), which was due to its high-elongation at break (higher than 350%) and negligible permanent set upon deformation. In contrast, the 3000M-85A had the maximum permanent set and minimum elongation at break, which caused the 3000M-85A PU to possess the lowest erosion resistance at 25 °C. On the other hand, at the set temperature of 60 °C, the erosion resistance of the 1200 series PU decreased due to the reduction of PU strength as a result of an increase in test temperature. Although the same behavior negatively affected the 3000 PU series, a greater ability to regain an initial state after deformation (smaller residual strain and higher Mullins factor value) led to the improvement in erosion resistance at that temperature. Finally, at the test temperature of 100 °C, the erosion rate of the 3000 series greatly increased due to the significant reduction in elongation at break of these PU elastomers. However, given that the permanent set of 3000M-85A at 100 °C was much smaller than the 3000-85A, its erosion resistance was not affected as severely as the 3000-85A PU. This behavior

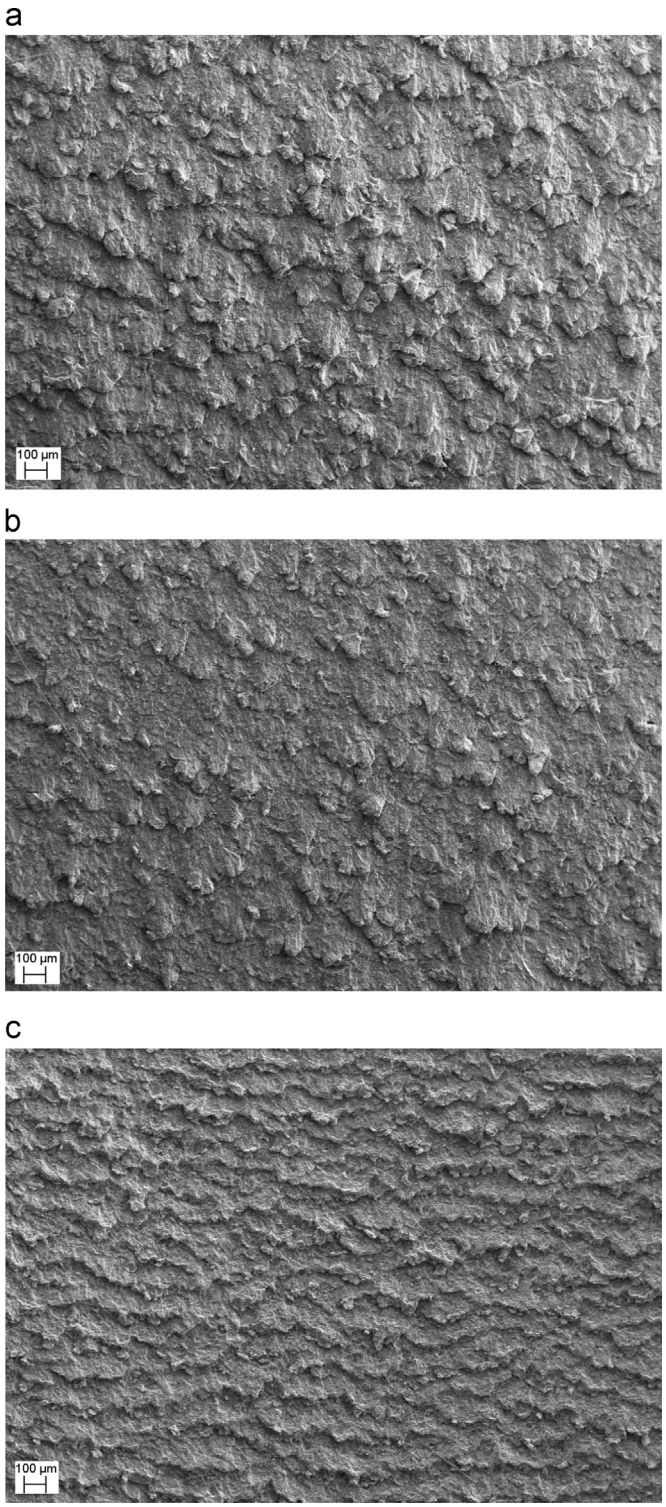

Fig. 12. SEM images of the eroded 3000-85A PU surface at (a) 25 °C, (b) 60 °C, and (c) 100 °C.

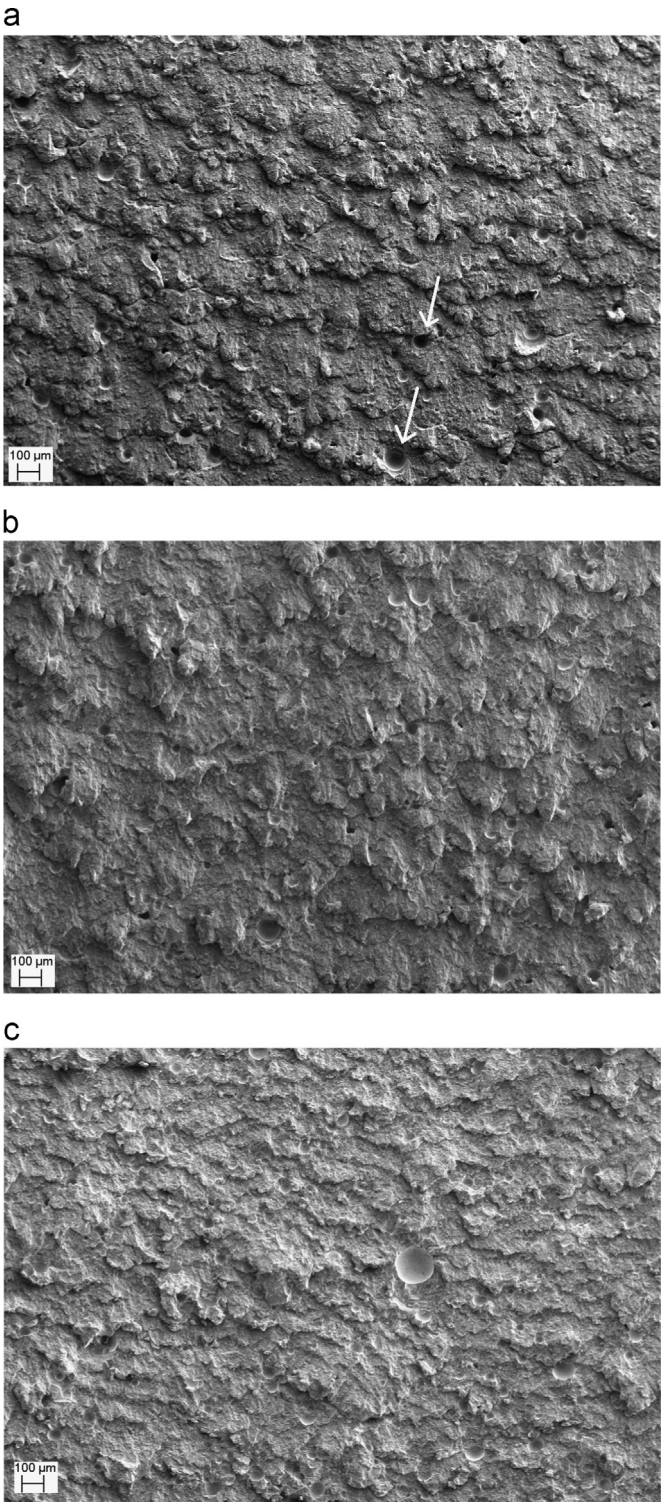

Fig. 13. SEM images of the eroded 3000M-85A PU surface at (a) 25 °C, (b) 60 °C, and (c) 100 °C.

further emphasizes the importance of the ability of a material to regain its initial state (smaller permanent set) on the wear resistance of PU elastomers. It should be noted that the basis for the given discussion is only the relative comparison of the erosion resistance of the studied PU elastomers and how the wear behavior is affected by the test temperature. A more in-depth comparison of the erosion rate of the studied PU elastomers is not possible given their differences in mechanical properties. Future work will be undertaken to develop models for calculating the generated stresses as a result of impacting erodant particles. The determination of stresses will allow for a more comprehensive comparison and explanation of what was observed for the erosion behavior shown in Fig. 5.

6. Conclusions

In this study, an erosion test assembly for evaluating the wear resistance of PU samples at controlled temperatures was designed

and developed. A cold gas dynamic spray system was used to enable the erosion tests. The velocity of the blast media was determined by the use of an analytical model based on the flow of a compressible gas through the cold spray nozzle. The temperature distribution within the PU samples during the erosion tests was computed employing a heat transfer model based on a finite element analysis. The model was validated by comparing the calculated temperature with the experimental data that was measured by a thermocouple. The calculated temperature distribution showed that the temperature in the area to be eroded was uniformly close to 60 °C and 100 °C for experiments conducted at elevated temperatures.

The evaluation of the wear resistance of PU elastomers at controlled temperatures showed that the PU elastomers do not generally exhibit similar behavior. Two of the tested PU elastomers showed improvement in erosion rate at 60 °C while the other studied elastomers exhibited an increase in erosion rate. At 100 °C, an increase in erosion rate for all studied PU elastomers was found. The evaluation of the mechanical properties of the studied PU elastomers suggested that the improvement in erosion rate at 60 °C was due to an improved ability of the material to regain its initial state following deformation. This behavior was studied by calculating the permanent set of the studied PU elastomers for cyclic loading. It was further found that although there is no simple relation between the elongation at break and erosion rate, it is definite that elongation at break is one of the parameters affecting the final wear resistance and the morphology of worn surfaces.

Besides studying the effect of working temperature on erosion performance of PU elastomers, this study allowed for a closer examination of erosion mechanisms for PU elastomers, and introduced the residual strain and elongation at break as key parameters affecting the PU elastomer wear resistance.

Acknowledgments

The authors would like to acknowledge the support by the Natural Sciences and Engineering Research Council of Canada (NSERC) (Grant no. CRDPJ 452584 – 13), Rosen Group and Syncrude Canada Limited. The authors would also like to thank Mr. Bernie Faulkner (Machine Shop, Department of Mechanical Engineering, University of Alberta) and Mr. Marcus Ivey (Multifunctional Fibrous Composites Laboratory, Department of Mechanical Engineering, University of Alberta) for their technical support.

References

[1] H. Ashrarfizadeh, F. Ashrafizadeh, A numerical 3D simulation for prediction of wear caused by solid particle impact, Wear 276–277 (2012) 75–84.
[2] P. Mertiny, K. Juss, T. Bell, Corrosion and erosion resistant polymer composite pipe for oil sands hydrotransport, in: Proceedings of the NACE International Corrosion Conference and Expo, New Orleans, LA, USA, 2008, Paper # 08667.
[3] N. Zhang, F. Yang, L. Li, C. Shen, J. Castro, L.J. Lee, Thickness effect on particle erosion resistance of thermoplastic polyurethane coating on steel substrate, Wear 303 (1–2) (2013) 49–55.
[4] J. Li, I.M. Hutchings, Resistance of cast polyurethane elastomers to solid particle erosion, Wear 135 (2) (1990) 293–303.
[5] J.C. Arnold, I.M. Hutchings, The mechanism of erosion of unfilled elastomers by solid particle impact, Wear 138 (1990) 33–46.
[6] Y. Xie, J. Jiang, K.Y. Tufa, S. Yick, Wear resistance of materials used for slurry transport, Wear 332–333 (2015) 1104–1110.
[7] F.J. Martinez, M. Canales, J.M. Bielsa, M.A. Jimenez, Relationship between wear rate and mechanical fatigue in sliding TPU–metal contacts, Wear 268 (2010) 388–398.
[8] K.G. Budinski, Guide to Friction, Wear and Erosion Testing, ASTM International, West Conshohocken, PA, USA, 2007.
[9] S.W. Zhang, W. Deguo, Y. Weihua, Investigation of abrasive erosion of polymers, J. Mater. Sci. 30 (1995) 4561–4566.
[10] Z. Ping, L. Youwei, Y. Chengqing, L. Jian, Erosion behaviors of polymer coatings, in: Proceedings of CST2008 & ITS-IFToMM, Beijing, China, 2008, pp. 738–741.
[11] P. Mertiny, R. Popella, K. Juss, Manufacturing of large-scale polyurethane-lined FRP piping, in: Proceedings of the ASME 2011 Pressure Vessels & Piping Division Conference, Baltimore, Maryland, USA, 2011, Paper # PVP2011-57870.
[12] R.A. Beck, R.W. Truss, Effect of chemical structure on the wear behavior of polyurethane-urea elastomers, Wear 218 (2) (1998) 145–152.
[13] I.M. Hutchings, D.W.T. Deuchar, Erosion of unfilled elastomers by solid particle impact, J. Mater. Sci. 22 (1987) 4071–4076.
[14] D.J. Hill, M.I. Kileen, J.H. O'Donnell, P.J. Pomery, D. John St., A.K. Whittaker, Laboratory wear testing of polyurethane elastomers, Wear 208 (1997) 155–160.
[15] N.M. Barkoula, J. Karger-Kocsis, Review processes and influencing parameters of the solid particle erosion of polymers and their composites, J. Mater. Sci. 37 (18) (2002) 3807–3820.
[16] F.J. Martinez, M. Canales, S. Izquierdo, M.A. Jimenez, M.A. Martinez, Finite element implementation and validation of wear modeling in sliding polymer–metal contacts, Wear 284–285 (2012) 52–64.
[17] S.W. Zhang, R. He, D. Wang, Q. Fan, Abrasive erosion of polyurethane, J. Mater. Sci. 36 (20) (2001) 5037–5043.
[18] Y.S. Zuev, A.D. Chelmodeev, Effect of temperature and concentration of aggressive media on rubber wear in an abrasive flow, MekP 4 (1) (1968) 95–101.
[19] A.I. Marei, P.V. Izvozchikov, Determination of the wear of rubbers in a stream of abrasive particles, in: D.I. James (Ed.), Abrasion of Rubber, Maclaren, London, England, 1967, pp. 274–280.
[20] ASTM G76, Standard test method for conducting erosion tests by solid particle impingement using gas jets, West Conshohocken, PA, USA, 2013.
[21] ASTM D638, Standard test method for tensile properties of plastics, West Conshohocken, PA, USA, 2014.
[22] R.C. Dykhuizen, M.F. Smith, Gas dynamic principles of cold spray, J. Therm. Spray Technol. 7 (1998) 205–212.
[23] M. Grujicic, C.L. Zhao, C. Tong, W.S. DeRosset, D. Helfritch, Analysis of the impact velocity of powder particles in the cold-gas dynamic-spray process, Mater. Sci. Eng. A368 (2004) 222–230.
[24] U. Prisco, Size-dependent distributions of particle velocity and temperature at impact in the cold-gas dynamic-spray process, J. Mater. Process. Technol. 216 (2015) 302–314.
[25] Y.T.R. Lee, H. Ashrafizadeh, G. Fisher, A. McDonald, effect of content and type of reinforcing particles on the hardness and wear rate of low-pressure cold-sprayed TiC and B4C-based metal matrix composite coatings, in: Proceedings of the International Thermal Spray Conference, Shanghai, China, 2016, pp. 310–315.
[26] H.Z. Li, J. Wang, J.M. Fan, Analysis and modelling of particle velocities in micro-abrasive air jet, Int. J. Mach. Tools Manuf. 49 (2009) 850–858.
[27] VV Mineral-Super Garnet Brochure, Retrieved from ⟨www.vvmineral.com/content/garnet-specification⟩, March 2016.
[28] ABAQUS Analysis User's Manual. Version 6. 7-EF1, Hibbitt, Karlsson & Sorensen Inc., 2007.
[29] L.M. Jiji, Heat Convection, second ed., Springer, Verlag Berlin Heidelberg, 2009.
[30] H. Ashrafizadeh, A. McDonald, P. Mertiny, Deposition of electrically conductive coatings on castable polyurethane elastomers by the flame spraying process, J. Therm. Spray Technol. 25 (2016) 419–430, http://dx.doi.org/10.1007/s11666-015-0376-2.
[31] C. Prisacariu, Polyurethane Elastomers – From Morphology to Mechanical Aspects, Springer, Verlag/Wien, 2011.
[32] X. Jia, R. Ling, Two-body free-abrasive wear of polyethylene, nylon1010, expoxy and polyurethane coatings, Tribol. Int. 40 (2007) 1276–1283.
[33] M. Yahiaoui, J. Denape, J.Y. Paris, A.G. Ural, N. Alcala, F.J. Martinez, Wear dynamics of a TPU/steel contact under reciprocal sliding, Wear 315 (2014) 103–114.
[34] J.C. Arnold, I.M. Hutchings, Flux rate effects in the erosive wear of elastomers, J. Mater. Sci. 24 (1989) 833–839.
[35] R.J.K. Wood, Y. Puget, K.R. Trethewey, K. Stokes, The performance of marine coatings and pipe materials under fluid-borne sand erosion, Wear 219 (1998) 46–59.